First remote measurements of lunar surface charging from ARTEMIS: Evidence for nonmonotonic sheath potentials above the dayside surface

J. S. Halekas,[1,2] G. T. Delory,[1,2] W. M. Farrell,[2,3] V. Angelopoulos,[4] J. P. McFadden,[1] J. W. Bonnell,[1] M. O. Fillingim,[1] and F. Plaschke[5]

Received 8 February 2011; revised 29 March 2011; accepted 21 April 2011; published 27 July 2011.

[1] During an early lunar encounter, ARTEMIS-P2 passed earthward from the Moon in the terrestrial magnetotail. Fortuitously, though more than 8000 km away, magnetic field lines connected the spacecraft to the dayside lunar surface during several time periods in both the lobe and plasma sheet. During these intervals, ARTEMIS made the first accurate and quantitative remote measurements of lunar surface charging from an observation point almost 100 times more distant than previous remote measurements of surface potentials. ARTEMIS also measured incident plasma, including hot tenuous electrons from a source deeper in the tail, portions of that population mirrored near the Earth, and cold ions from the terrestrial ionosphere. The spatial and temporal variation of these sources, combined with shadowing by the lunar obstacle and motion and curvature of magnetotail field lines, leads to highly variable charging currents to the surface. ARTEMIS measurements provide evidence for negative dayside surface potentials, likely indicative of nonmonotonic sheath potentials above the sunlit surface, in the plasma sheet and, for the first time, in the tail lobe. These nonmonotonic potentials, and the resulting accelerated outward going beams of lunar photoelectrons, may help maintain quasi-neutrality along magnetic field lines connected to the Moon.

Citation: Halekas, J. S., G. T. Delory, W. M. Farrell, V. Angelopoulos, J. P. McFadden, J. W. Bonnell, M. O. Fillingim, and F. Plaschke (2011), First remote measurements of lunar surface charging from ARTEMIS: Evidence for nonmonotonic sheath potentials above the dayside surface, *J. Geophys. Res.*, *116*, A07103, doi:10.1029/2011JA016542.

1. Introduction

[2] The lunar surface, unprotected by a significant atmosphere or a global magnetic field, lies exposed to incident plasma of solar and/or terrestrial origin, as well as solar photons and other external influences, all with properties that vary widely over the course of the lunar orbit and the solar cycle. As a result, the Moon provides an ideal environment for studying the dynamics of a number of fundamental plasma physics processes, as reviewed by *Halekas et al.* [2010], including surface charging and plasma sheath formation. These processes control the near-surface electromagnetic environment, and may also therefore prove relevant for exploration.

[3] Lunar surface charging, much like spacecraft charging, has often been treated as a simple current balance problem, wherein the surface floats to an electrostatic potential at which currents corresponding to incident electrons and ions, escaping photoelectrons and secondary electrons, and any other current sources, balance [*Whipple*, 1981; *Manka*, 1973]. Over most of the sunlit hemisphere, one expects photoemission to dominate, driving the surface to a positive potential on the order of +5–10 V. On the night side, on the other hand, electron thermal currents generally dominate, driving the surface to a negative potential on the order of the electron temperature (except in cases with significant secondary electron emission). Measurements from both the lunar surface and orbit have largely supported the conclusions of such current balance analyses for the Moon, especially in shadow [*Freeman and Ibrahim*, 1975; *Halekas et al.*, 2008].

[4] However, in sunlight, particularly in the terrestrial magnetosphere, several measurements potentially relevant to lunar surface charging have proven difficult to interpret. In the low-density terrestrial magnetotail lobe, electron measurements at the surface [*Reasoner and Burke*, 1972] and ion measurements in orbit [*Tanaka et al.*, 2009] have at times provided tentative evidence for rather large positive surface potentials on the order of a few hundred volts, though the interpretation of both of these measurements

[1]Space Sciences Laboratory, University of California, Berkeley, California, USA.
[2]NASA Lunar Science Institute, Ames Research Center, Moffett Field, California, USA.
[3]NASA Goddard Space Flight Center, Greenbelt, Maryland, USA.
[4]Institute of Geophysics and Planetary Physics, University of California, Los Angeles, California, USA.
[5]Institut für Geophysik und Extraterrestrische Physik, Technische Universität Braunschweig, Braunschweig, Germany.

0148-0227/11/2011JA016542

remains uncertain. On the other hand, during many time periods in the plasma sheet, Lunar Prospector (LP) data provides evidence for large negative dayside surface potentials, even during periods when the expected photoemission currents greatly exceed plasma currents [*Halekas et al.*, 2005, 2008]. LP observations rely on two indicators as diagnostics of negative lunar surface charging. First, downward electric fields below the spacecraft lead to energy-dependent electron reflection, with the shape of the electron loss cone related to the total potential drop between the spacecraft and the surface. Second, downward electric fields accelerate low energy secondary electrons and/or photoelectrons produced at the surface upward, producing a beam with an energy corresponding to the total potential drop between the spacecraft and the surface. LP measurements suffer from unavoidable measurement errors, given the lack of spacecraft potential knowledge, but prove difficult to interpret in any other manner than negative dayside surface charging [*Halekas et al.*, 2008].

[5] One possible explanation for the LP results comes from a variety of theoretical work [*Guernsey and Fu*, 1970; *Nitter et al.*, 1998] and simulations [*Poppe and Horányi*, 2010; *Ergun et al.*, 2010] demonstrating that, at least for some conditions, the favored potential distribution above a sunlit surface has a nonmonotonic profile with altitude. In this case, a potential minimum formed by space charge above the surface reflects most incident electrons and traps most photoelectrons near the surface, allowing the surface to float to anomalously large negative values compared to those predicted by a simple current balance calculation. Just as in a typical photoelectron sheath, the sunlit surface has a more positive potential than the near sheath; however, in the nonmonotonic case the sunlit surface can reach a negative potential relative to the ambient plasma, thanks to the shielding effect of the potential barrier produced by space charge (this barrier sits at a slightly more negative potential than the surface). The observational signature of negative surface charging, meanwhile, should remain much the same as that above a monotonic sheath, as long as the potential barrier remains small enough that it does not trap all electrons produced at the surface.

[6] Spacecraft charging simulations predict that such nonmonotonic potential layers should occur preferentially above objects much larger than the Debye scale, for photoelectron densities much larger than electron densities, and for electron thermal energies much larger than the photoelectron temperature [*Ergun et al.*, 2010]. The lunar surface, especially in the terrestrial magnetosphere, very often satisfies all of these criteria; therefore, one may expect this situation to occur quite commonly at the Moon. Indeed, particle-in-cell (PIC) simulations predict nonmonotonic potentials above the sunlit lunar surface in many plasma regimes, including the solar wind and plasma sheet [*Poppe and Horányi*, 2010; *Poppe et al.*, 2011].

[7] Preliminary comparisons of PIC model results with plasma sheet data from LP show very encouraging consistency, lending credence to the existence of nonmonotonic potentials above the dayside surface in at least one plasma regime [*Poppe et al.*, 2011]. Solar wind data also provide hints of such structures, though LP did not have energy resolution and coverage sufficient to make definitive conclusions [*Halekas et al.*, 2011]. The terrestrial magnetotail lobes, meanwhile, which have plasma densities so low ($<\sim 0.1$ cm^{-3}) that spacecraft charge to rather large positive potentials and spacecraft photoelectrons dominate measurements, present a very difficult environment in which to remotely measure surface charging. LP's limited (~50%) energy resolution and the lack of a spacecraft potential measurement ensured that it could not separate ambient electrons from spacecraft photoelectrons well enough to do more than provide rough limits, which suggested surface potentials more positive than ~–20 V [*Halekas et al.*, 2008]. Therefore, the existence of nonmonotonic potentials above the dayside lunar surface in the tail lobes remained an open question prior to the ARTEMIS mission.

[8] The two-probe ARTEMIS mission [*Angelopoulos*, 2010], with full plasma instrumentation, much better (17% intrinsic, binned at 32%) electron energy resolution, and measurements of spacecraft potential, now provides an opportunity to make the first accurate and quantitative measurements of lunar surface potentials from orbit, as well as the incident plasma populations that drive lunar surface charging. In this paper, we present the first measurements of lunar surface charging from ARTEMIS-P2, during an early flyby on 28 March 2010 that took place over 8000 km earthward from the lunar surface, in the terrestrial magnetotail. Despite its position nearly one hundred times farther from the Moon than LP, ARTEMIS measured secondary and/or photo-emitted electrons accelerated from the sunlit lunar surface along magnetic field lines connected to the Moon, indicating negative surface potentials on the order of the electron temperature in both the tail lobe and plasma sheet, in agreement with previous predictions of nonmonotonic potential profiles above the lunar dayside.

2. ARTEMIS-P2 Lunar Encounter in the Terrestrial Magnetotail

[9] Figure 1 shows an overview of the lunar encounter in question, which took place near the flanks of the terrestrial magnetotail at an average GSE position of [−49, 24, −4] R_E. Just after 7:00 UT, ARTEMIS made its closest approach of ~10,000 km from the center of the Moon, or slightly more than ~8000 km earthward from the dayside surface (R_M = 1738 km). Centered on the time of this closest approach, extending from 06:26–07:38, ARTEMIS collected particle burst data (as seen in the higher time resolution of the electron and ion energy spectra), enabling the collection of many individual measurements of lunar surface charging. Before 7:15, the ESA [*McFadden et al.*, 2008] and FGM [*Auster et al.*, 2008] instruments measured plasma and magnetic fields characteristic of the geomagnetic tail lobes. After 7:15, ARTEMIS observed plasma and fields consistent with a transition through the plasma sheet boundary layer (PSBL) into the plasma sheet. Throughout this time period, the spacecraft floated to large positive potentials characteristic of tenuous plasma environments, with the spacecraft potential measured by the EFI instrument [*Bonnell et al.*, 2008] marking the boundary in the measured electron energy spectra separating ambient electrons from high fluxes of spacecraft photoelectrons.

[10] Large spacecraft potentials make electron moment calculations difficult, since the spacecraft potential accelerates electrons into the instrument and thereby degrades the effective energy resolution for low energy electrons. As a result, the position of the spacecraft potential relative to the

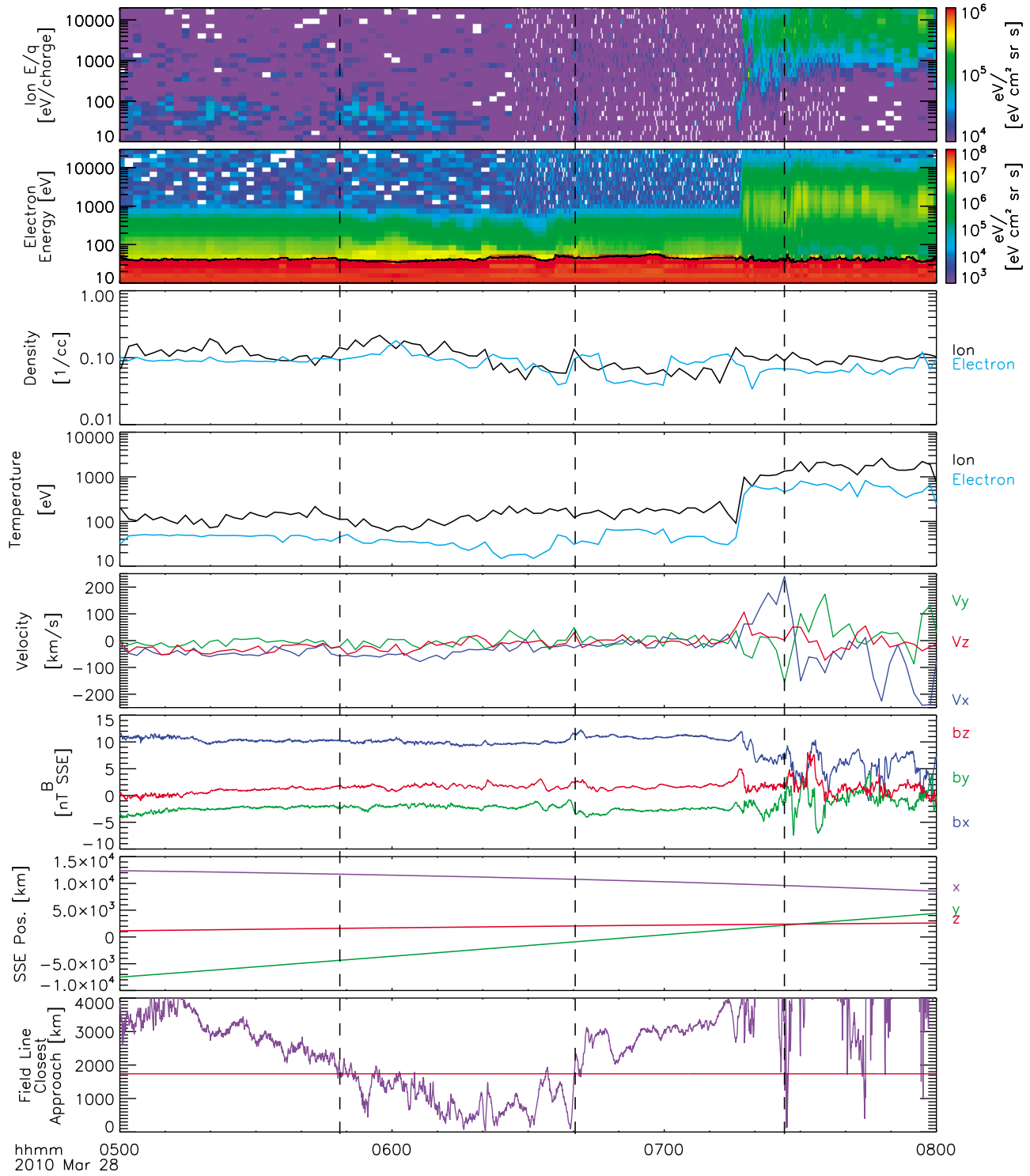

Figure 1. Overview of ARTEMIS-P2 lunar flyby in terrestrial magnetotail on 28 March 2010, with ion energy/charge spectra, electron energy spectra, background-subtracted density and temperature moments for ions (black) and electrons (blue), ion velocity moments, magnetic field and spacecraft position in SSE (Selenocentric Solar Ecliptic) coordinates, and the closest approach of a straight-line extrapolation of the measured magnetic field vector to the center of the Moon (red line indicates lunar radius; thus, values below this line imply magnetic connection to the lunar surface). Black curve on electron spectrogram indicates the spacecraft potential. Dashed lines indicate magnetically connected intervals discussed in more detail below.

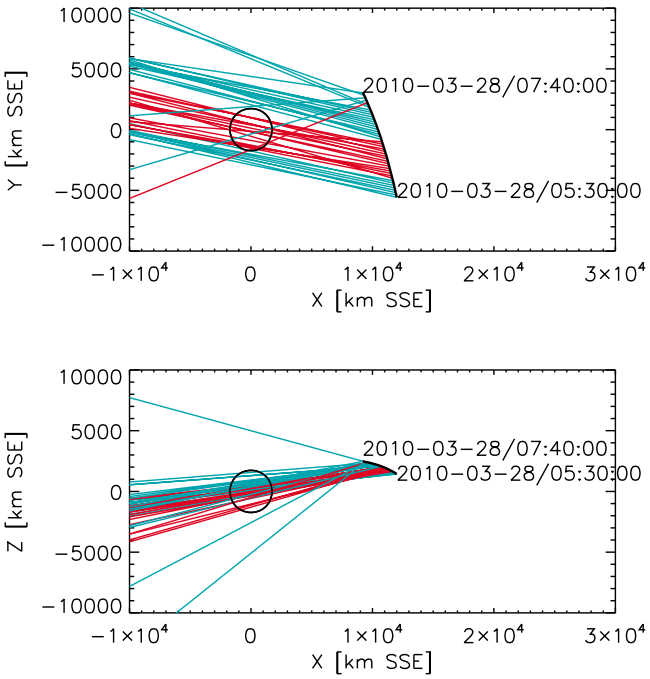

Figure 2. ARTEMIS-P2 trajectory in SSE coordinates during lunar flyby, with straight-line moonward extrapolations of measured magnetic field vectors from the spacecraft (red is connected, blue is unconnected) plotted every 180 s.

boundaries of ESA energy bins (now broad compared to the real energy of electrons prior to acceleration into the instrument) can affect the moment calculation. Because of this, in sections 3 and 4, we elect to fit to electron distributions rather than relying on moments to determine critical electron parameters. Meanwhile, in the tail lobe the positive spacecraft potential also hindered ESA's ability to measure cold ions, by repelling them from the spacecraft, leaving little but background counts in ion spectra, and leading to likely underestimates of ion density. During some time periods in the lobe (5:00–5:35, 5:45–6:22, 6:40–6:42), thanks to increases in ion flow speed, ESA measured some tenuous low energy ions despite the large positive spacecraft potential. In the plasma sheet, both ion temperature and flow velocity increase dramatically, allowing ESA to measure all low energy ions; however, at these times the ion energy spectrum extends to energies above the ESA energy range, again leading to probable underestimates of ion density. Despite these various caveats, electron and ion density moments agree to within ~50% throughout the encounter, and indicate very low plasma densities <~0.1 cm^{-3}.

[11] For most of the time period from 5:48–6:40 in the lobe (delineated by first two dashed lines on Figure 1), and for a few short time periods (one at ~7:27 shown with third dashed line) in the plasma sheet, a straight-line extrapolation of the measured magnetic field vector from the spacecraft indicates that it should connected to the lunar surface, as indicated in the eighth panel of Figure 1. Magnetic connection to the Moon proves extremely important in determining the motion of electrons, since the gyroradius of even the most energetic electrons observed during this time period is less than ~30 km, orders of magnitude smaller than the Moon. Figure 2 shows the details of the encounter geometry and inferred magnetic connection, assuming no magnetic field curvature. During the lobe portion of the flyby, the magnetic field geometry remains nearly constant, with nearly continuous connection to the surface as the spacecraft traverses the flux tubes intersecting the Moon. Later, in the plasma sheet, magnetic field geometry varies rapidly, and a straight-line magnetic field trace predicts a brief period of magnetic connection as the field line measured at the spacecraft swings across the Moon.

[12] Ambient plasma in the terrestrial magnetotail may have a number of sources, leading to temporally and spatially variable charging currents to the surface, as shown in Figure 3. First, plasma outflows from the terrestrial ionosphere produce a population of cold plasma difficult to observe, but often present, in the magnetotail. On open field lines connected to the Moon, this tailward flowing plasma will impact the lunar dayside surface; on closed field lines (not shown in Figure 3) it could impact the dayside or nightside hemisphere. The tailward flowing ions seen early in the lobe portion of the encounter, and perpendicularly accelerated cold ions observed near the PSBL (discussed further in section 4), may belong to this terrestrial population. Next, hotter plasma produced by reconnection and other acceleration processes or modified from incoming solar wind populations can have sources earthward or farther down the tail from the Moon, depending on magnetotail topology. Sources of warm plasma earthward of the Moon (not shown in Figure 3) should have incidence patterns similar to that of cold terrestrial plasma, but larger temperatures.

[13] Sources father down the tail from the Moon, on the other hand, produce warm plasma that will mostly impact the nightside surface. However, if magnetotail field lines move laterally, earthward going plasma on flux tubes moving past the Moon can also bypass the Moon, mirror near the Earth, and impact the dayside surface, with access to the dayside for this population depending on particle energy (and therefore mirroring time) and field line convection velocity. The motion of field lines, coupled with the removal of charged particles that impact the lunar surface, can therefore lead to energy-dependent bidirectional shadowing of plasma near the Moon, a phenomenon previously used to infer magnetotail convection velocities [*Anderson and Lin*, 1969]. We will discuss indications of such shadowing, suggesting a warm plasma source down the tail from the Moon during this encounter, in section 3.

3. Tail Lobe Observations

[14] Figure 4 shows an overview of the tail lobe portion of the encounter, focusing first on the properties of the ambient electrons incident on the Moon. The top four panels show the properties of moonward going electrons, including energy spectra of electrons with pitch angles of 165°–180°, and density and temperature parameters derived from Maxwellian fits to these moonward spectra. The resulting fit parameters describe only moonward going electrons, and do not necessarily correspond to bulk properties. Next, we derive the thermal electron current to the lunar surface by assuming an isotropic distribution with these same fit parameters, but extending over the entire velocity half-space containing particles incident on the Moon. Checks of angular

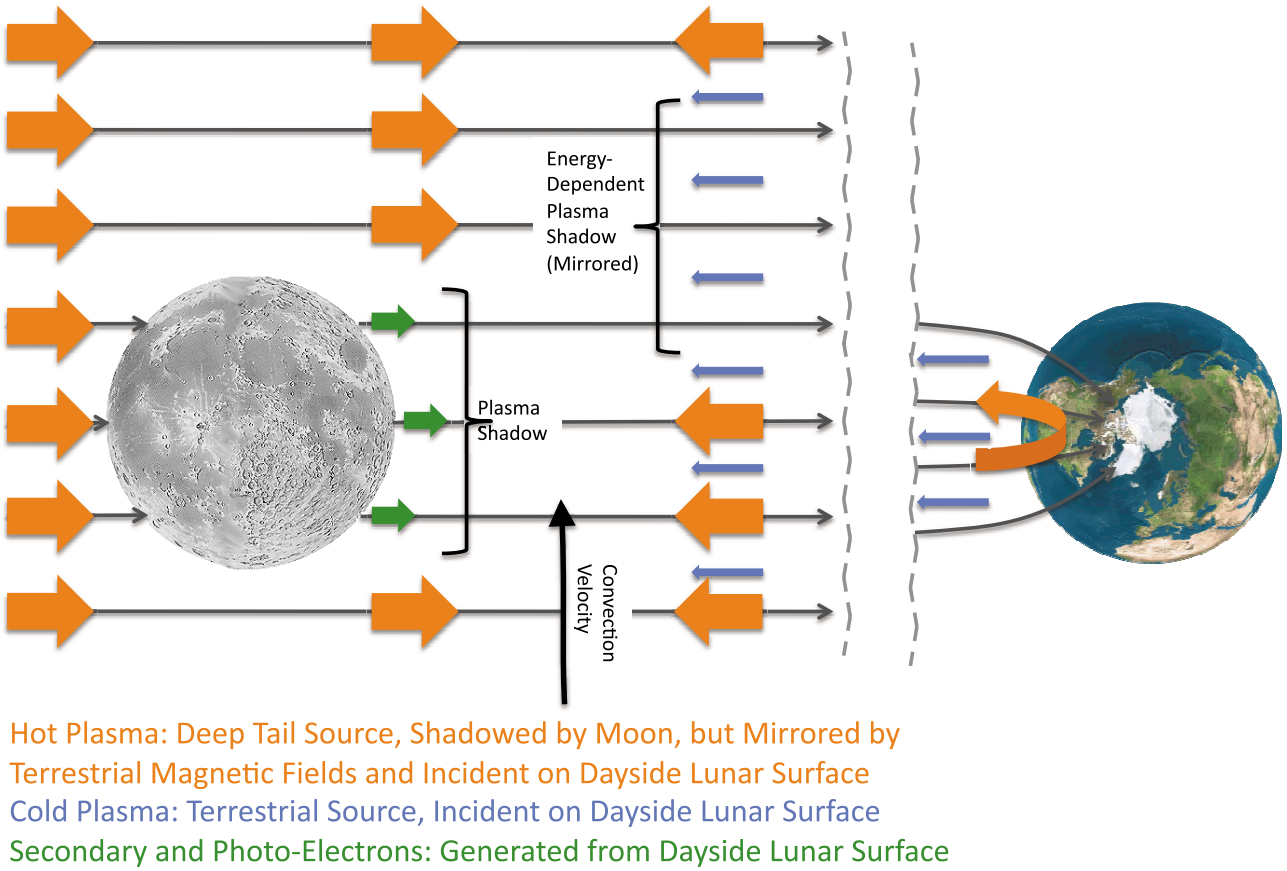

Figure 3. Schematic overview of plasma sources in the *cis*-lunar environment in the terrestrial magnetotail during the ARTEMIS-P2 lunar flyby, assuming open magnetic field lines and a tailward source of hot plasma.

distributions (see, e.g., Figures 5 and 7) show that the observed moonward going electrons roughly satisfy this assumption of isotropy, validating our approach. The current to the surface so derived lies over two orders of magnitude below the expected photoemission current from the surface [*Feuerbacher et al.*, 1972; *Willis et al.*, 1973], even taking into account the reduction of photoemission at high solar zenith angles (SZA). Therefore, a current balance analysis would predict significant positive surface charging, much like that observed for the ARTEMIS spacecraft. However, we will see that the observations do not support this expectation.

[15] Several features in the moonward electron spectra help us determine the sources of ambient electrons. For much of the magnetically connected interval, plasma incidence on the dayside surface continues unabated, which could indicate either sources of plasma earthward from the Moon, or field line motion fast enough to prevent flux tubes from emptying before moving past the Moon. However, during four connected intervals (5:56–5:58, 6:14–6:16, 6:17–6:20, 6:28–6:35) we observe depletions of moonward flux, consistent with magnetic connection long enough for plasma to evacuate the connected flux tubes (only possible if the ultimate source of plasma lies farther down the tail from the Moon). For the latter three times, this depletion roughly follows a dispersion curve in energy versus time (for the first two, only a partial dispersion curve), approximately matching the expected travel time for electrons of a given energy to travel into the strong near-Earth magnetic field, mirror, and return to the Moon. Thus, these represent time periods when magnetic flux tubes connect to the dayside lunar surface long enough to empty of electrons. The inferred ~6–7 min duration of magnetic connection for the last of these times implies perpendicular field line motion at velocities <~10 km/s at these times, a relatively slow convection speed not directly measurable by most instrumentation.

[16] Note that low energy electrons produced from the lunar surface could also mirror and return to the Moon during a sufficiently long (several minutes) connection period; indeed, at the end of the last dispersion period (6:32–6:35), we note an increase in low energy electron flux, possibly indicating just such a returning population. Note that such a mirrored population would probably no longer have a purely beamlike nature, since instabilities might smooth out the distribution on more rapid timescales than the mirroring time. However, the bulk of the population could still return to the Moon, albeit in a more relaxed form. If correct, this implies that we can think of the Moon as a weak source of low-energy plasma that could impact the near-Earth environment, similar to many outer planet moons. For particularly energetic times, one could even imagine these electrons producing auroral signatures, in analogy to the outer planet case. In addition, the portion of this low energy population that mirrors near the Earth can then return to the lunar environment, potentially producing interesting feedback effects.

[17] Next, in the sixth and seventh panels of Figure 4, we investigate earthward electron spectra, and the ratio between earthward and moonward spectra. We find that the energetic earthward electron fluxes drop out when a straight-line field trace intersects the lunar surface, with very good correlation, consistent with the blockage of earthward flux by the lunar obstacle. Earthward flux does recover at four times (5:57–5:58, 5:59–6:02, 6:34–6:35, 6:37–6:38), with the first three recoveries almost perfectly corresponding to times when a straight-line trace predicts disconnection, and the last one at a time with only glancing connection predicted. The last recovery does not quite agree with predictions from a straight-line trace, likely indicating slight field line curvature.

[18] During all magnetically connected times, when we observe an earthward flux dropout, we also see an earthward going beam of electrons at energies just above the spacecraft potential (less well resolved in lower angular resolution reduced data before ~6:26, but still clearly present, and

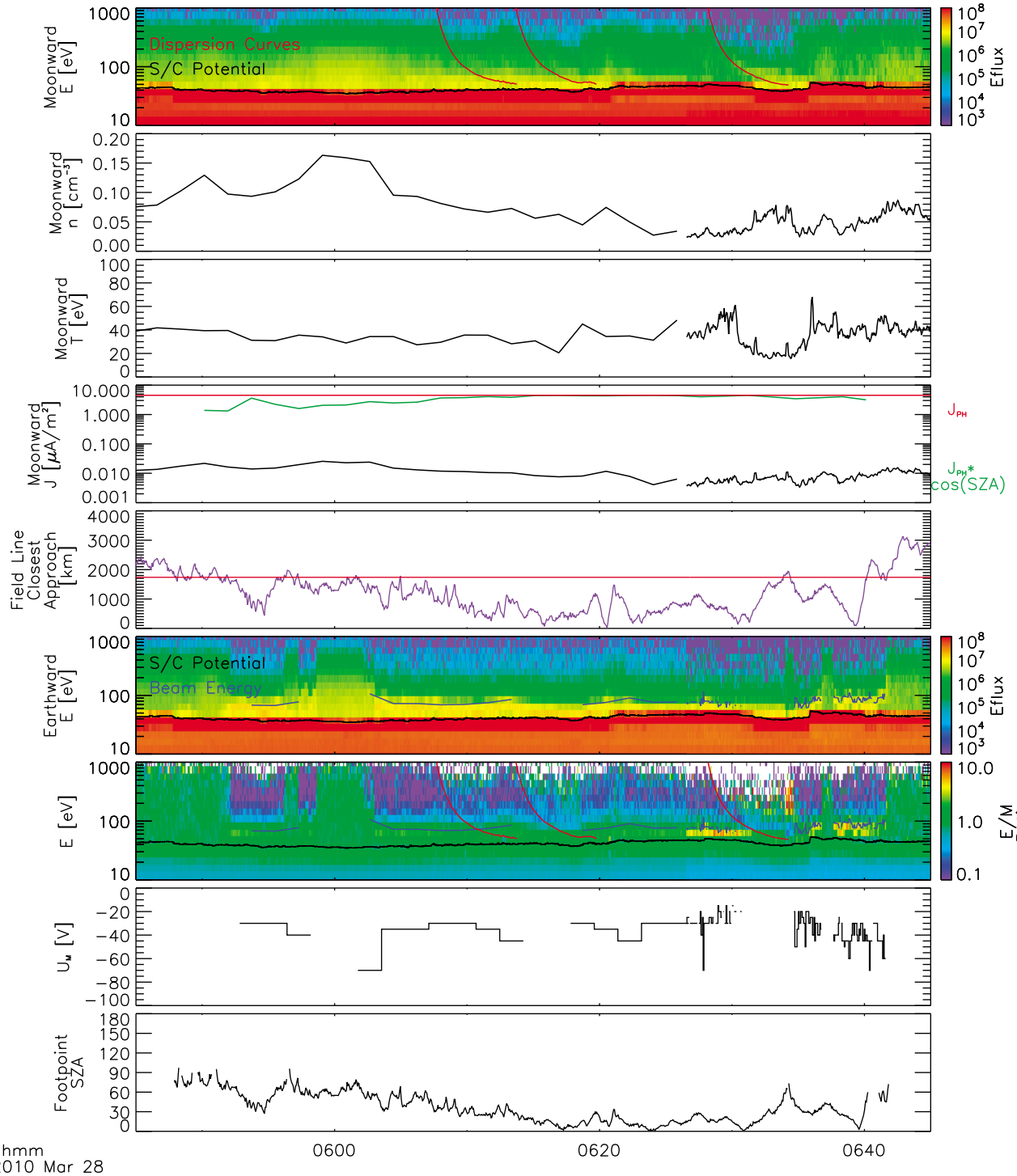

Figure 4

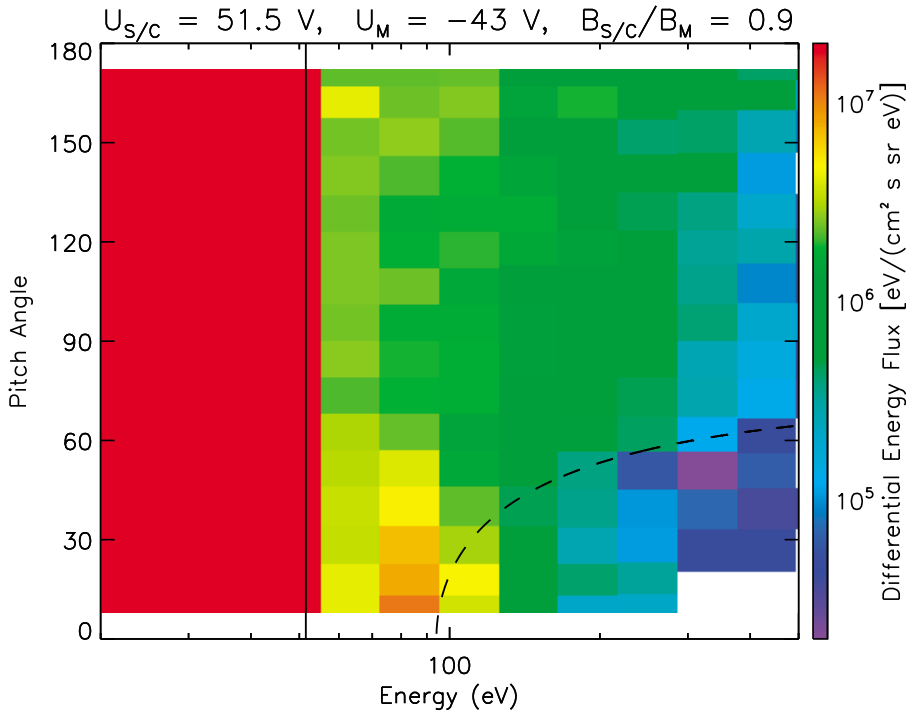

Figure 5. ARTEMIS-P2 electron data taken at 6:37:45, during a magnetically connected interval in the tail lobe. Dashed line indicates a loss cone of the form $\sin^2 \alpha_c = (B_{S/C}/B_M)(13 + eU_M/E)$, as determined from the best fit to a synthetic distribution that includes both the energy-dependent loss cone and the accelerated secondary beam. The solid line shows the measured spacecraft potential $U_{S/C}$, which introduces an energy shift to the function above that we remove before fitting.

easily seen in full angular resolution data at lower time resolution), traveling outward from the dayside lunar surface. This beam has higher flux than incident electrons at the same energy, and cannot represent electrons adiabatically reflected by either crustal magnetic fields or electric fields. Instead, the beam likely results from low energy secondary and/or photoelectrons produced at the surface and accelerated outward by a downward electric field above the surface, just as often observed above the nightside lunar surface [*Halekas et al.*, 2008]. Given the low ratio of incident electron current to the expected photoelectron current, negative surface potentials cannot result from simple current balance. Instead, a nonmonotonic potential distribution above the surface provides the most likely explanation for these observations. These observations therefore provide the first indication that nonmonotonic potential structures can form above the dayside lunar surface in the tail lobe, as well as in the plasma sheet where we have previously observed similar features [*Poppe et al.*, 2011].

[19] We utilize existing software tools that fit to the entire electron angular distribution, including both the energy-dependent loss cone and the upward going beam, to determine the lunar surface potential [*Halekas et al.*, 2008]. These tools, first used to analyze LP Electron Reflectometer (ER) data taken at low altitudes of ~30–100 km, work equally well at the much larger distance of ARTEMIS-P2 at this time. As described by *Halekas et al.* [2008], we normalize each measured distribution (both downward going and upward going halves) by the incident portion of the distribution, thereby creating a relative reflection/emission

Figure 4. Overview of magnetically connected interval in the Earth's tail lobe, with moonward (pitch angles 165°–180°) electron energy spectra and moonward density, temperature, and current to surface from Maxwellian fits (with estimated photoelectron current for comparison), closest approach of extrapolated field line position, earthward (pitch angles 0°–15°) electron energy spectra, ratio of earthward to moonward electron energy spectra, inferred lunar surface potential, and field line foot point solar zenith angle. All electron energy spectra before 6:26 use reduced data with somewhat lower angular resolution to obtain higher time resolution; however, calculations of moments and lunar surface potential use data with full angular resolution but lower time resolution. Red dispersion curves on moonward and ratio spectrograms show the time for particles to travel 120 R_E, or roughly the time for particles to travel into the Earth's magnetic field, mirror, and return to the Moon. If the start time indicates the time at which a given flux tube first intersected the Moon, the dispersion curves represent the time for particles with the given energies to completely evacuate the flux tube. Blue beam energy curves on earthward and ratio spectrograms show the energy of a secondary particle accelerated from the lunar surface with the inferred lunar potential and postaccelerated by the measured spacecraft potential. Black curves on all electron spectrograms indicate the spacecraft potential.

distribution as a function of energy and pitch angle. We then create a range of synthetic distributions to try to match this normalized distribution, with each including both the secondary electron beam and the energy-dependent loss cone (corrected for spacecraft potential). We then find the best match, using a least squares fit metric, to the observed distribution in order to simultaneously constrain the lunar surface potential and the magnetic field ratio. For ease of analysis, we assume that the surface potential U_M and the minimum potential along the field line U_{Min} are equal. For a monotonic potential this holds exactly, while for a nonmonotonic potential simulation results [*Poppe et al.*, 2011] indicate that neglecting the small difference between the potential at the surface and at the minimum should prove a reasonable approximation at the ~10% level. We show an example of the output of this analysis in Figure 5. We see that our fitting procedure converges on a surface potential and magnetic field ratio corresponding to a consistent secondary beam and energy-dependent loss cone. The loss cone fits the measured data over a broad range of electron energies, lending confidence in our analysis and interpretation. Since the measurements have an offset due to post-acceleration of electrons by the spacecraft potential, all remote measurements of lunar surface potential depend critically on knowledge of the spacecraft potential. With ARTEMIS, for the first time we have an accurate measurement of this crucial parameter, thereby removing a large unknown offset in all previous remote measurements of lunar surface charging.

[20] Analyzing all ARTEMIS electron data with full angular resolution collected during this time interval in the same manner described above, we find lunar surface potentials of −30 to −60 V, on the order of the electron temperature, as expected from previous simulations [*Poppe et al.*, 2011]. Note that our procedure does not always find a beam, since it has defined thresholds for identification, resulting in some small gaps in surface potential determinations. We find little clear dependence on the solar zenith angle of the surface where the magnetic field line intersects, likely indicating that photoelectron emission even near the flanks remains strong enough compared to plasma currents to drive the sheath to a nonmonotonic state. However, the large positive spacecraft potential, which degrades the electron energy resolution at the low end, limits our ability to precisely measure the electron beam energy. We discuss faint statistical hints of a tendency for smaller negative potentials at lower solar zenith angle in more detail in section 5.

4. Plasma Sheet Observations

[21] Figure 6 shows an overview of the plasma sheet portion of the encounter, in a very similar format to that in Figure 4. As above, we first focus on the moonward electrons capable of impacting the dayside lunar surface (not all of which do so, given the limited magnetic connection). The moonward electron density remains nearly constant over this interval, and roughly the same as in the tail lobe portion of the encounter. However, at 7:17, we see a large increase in electron temperature, characteristic of an entry into the plasma sheet. The increased temperature drives a corresponding increase in the predicted thermal electron current to the surface; however, this current remains almost two orders of magnitude below the expected photoelectron current. Therefore, a current balance calculation would again predict positive lunar surface potentials.

[22] Nonetheless, during a brief period of magnetic connection at 7:27, we again observe a dropout in earthward electron flux at most energies, coincident with a high flux beam of electrons traveling out from the lunar surface, consistent with magnetic connection to a negatively charged lunar surface. We conduct the same analysis as in section 3, showing an example in Figure 7, and find lunar surface potentials of −180 to −450 V, again on the same order as the electron temperature of 400 eV, in agreement with previous studies of dayside charging in the plasma sheet [*Poppe et al.*, 2011]. ARTEMIS data therefore provides corroborative evidence for the existence of nonmonotonic potentials above the dayside surface in the plasma sheet, but now affords accurate determinations of the magnitude of those potentials, with no unknown offset due to spacecraft charging as in previous studies. The more comprehensive plasma measurements from ARTEMIS should allow a more thorough study of the effect of initial conditions (for example, ion temperature) on the structure of this sheath potential. As an aside, we note that the secondary beam in Figure 7 appears much wider in both energy and angle than expected for an accelerated cold secondary population, most likely indicating the effect of potentially interesting beam-plasma instabilities between the lunar surface and the ARTEMIS location, which should also be investigated in future work.

[23] The brief interval of magnetic connection and its relation to measured plasma conditions deserves some additional discussion. The beginning of the connected interval corresponds perfectly with predictions from a straight-line field trace; however, the connected interval extends ~30 s beyond the straight-line prediction. One can attempt to explain this discrepancy in terms of either field line motion or curvature. First, we consider field line motion, which we fortuitously have a direct measure of. Just before the entry into the plasma sheet, we observe a low energy population of ions concentrated at angles perpendicular to the field line. These perpendicular ion signatures, often seen in and near the PSBL [*Hirahara et al.*, 1994], represent cold ions $\dot{\boldsymbol{E}} \times \dot{\boldsymbol{B}}$ drifting perpendicular to the magnetic field-in other words, co-moving with the field line. This cold population likely has a terrestrial origin, and persists throughout the lunar encounter (one could consider a lunar origin for the cold ions, but we find the highly variable inferred field line connection and motion impossible to reconcile with a lunar origin for ions seen over such a long time interval). Whenever the perpendicular field line velocity increases above ~100 km/s, ARTEMIS can measure this cold population. In the ninth panel of Figure 6 we show energy spectra for ions traveling perpendicular to the field. These perpendicular ions have both a high-energy component belonging to a fairly isotropic hot population, and a low-energy component corresponding to the cold drifting ions. We calculated the perpendicular ion velocity moment using several different energy windows, and found that the perpendicular velocity of the hot and cold components agree well, supporting the interpretation of field line convection. We show the perpendicular velocity determined from the drifting population in the tenth panel of Figure 6, and overplot the energy corresponding to that

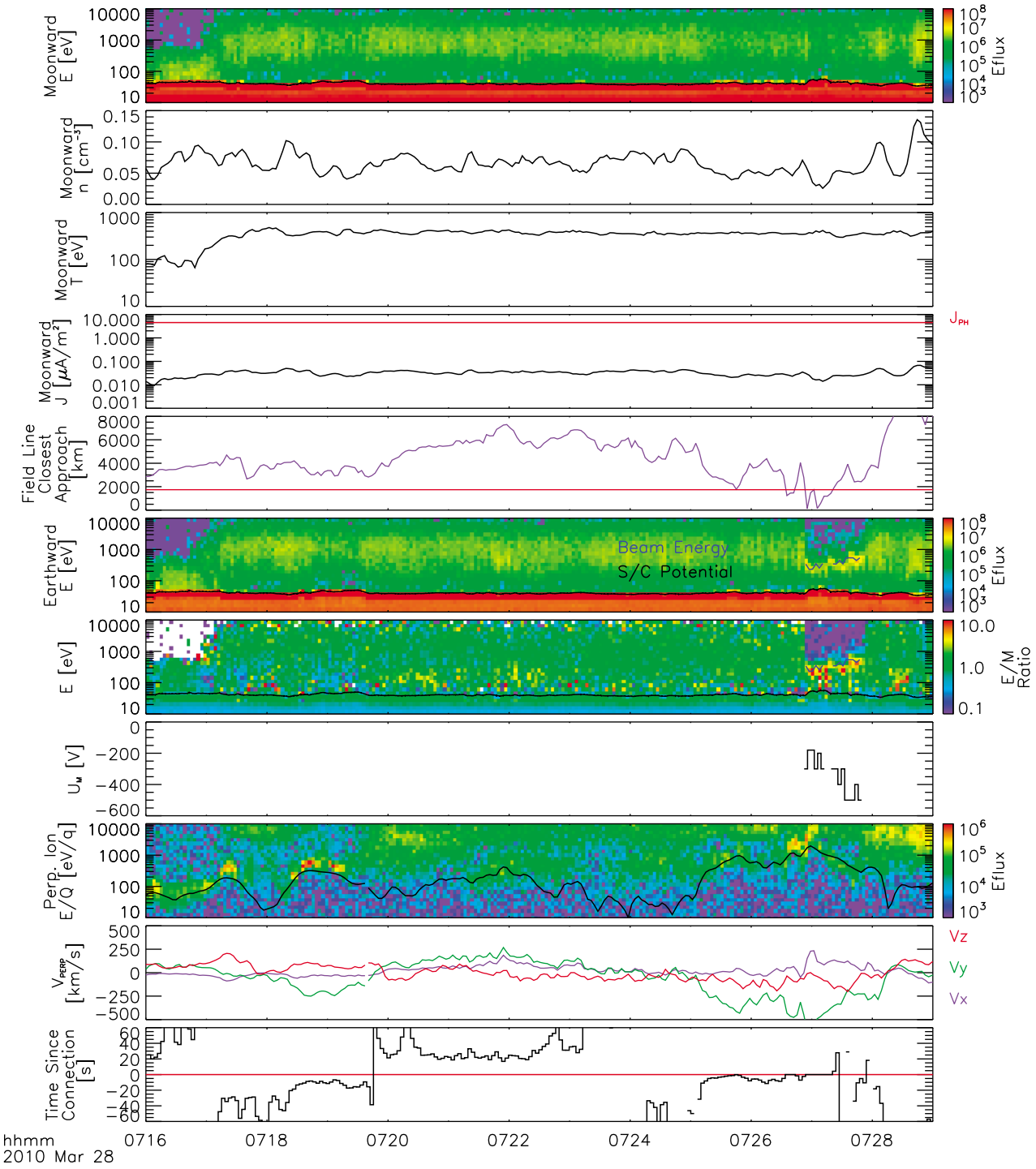

Figure 6. Overview of time period around magnetically connected interval in the Earth's plasma sheet/plasma sheet boundary layer, with moonward (pitch angles 165°–180°) electron energy spectra and fitted density, temperature, and current to surface (with estimated photoelectron current for comparison), closest approach of extrapolated field line position, earthward (pitch angles 0°–15°) electron energy spectra, ratio of earthward to moonward electron energy spectra, inferred lunar surface potential, perpendicular (pitch angles 70°–110°) ion energy spectra, perpendicular ion velocity from partial moment analysis, and time since magnetic field connection to the Moon (assuming no field line curvature or rotation; negative values indicate field lines that have never been connected to the Moon, given these assumptions). Black curve overlaid on perpendicular ion spectrogram indicates the energy of an ion traveling with the derived perpendicular ion velocity. Blue beam energy curves on earthward and ratio spectrograms show the energy of a secondary particle accelerated from a surface with the inferred lunar potential and postaccelerated by the measured spacecraft potential. Black curves on all electron spectrograms indicate the spacecraft potential.

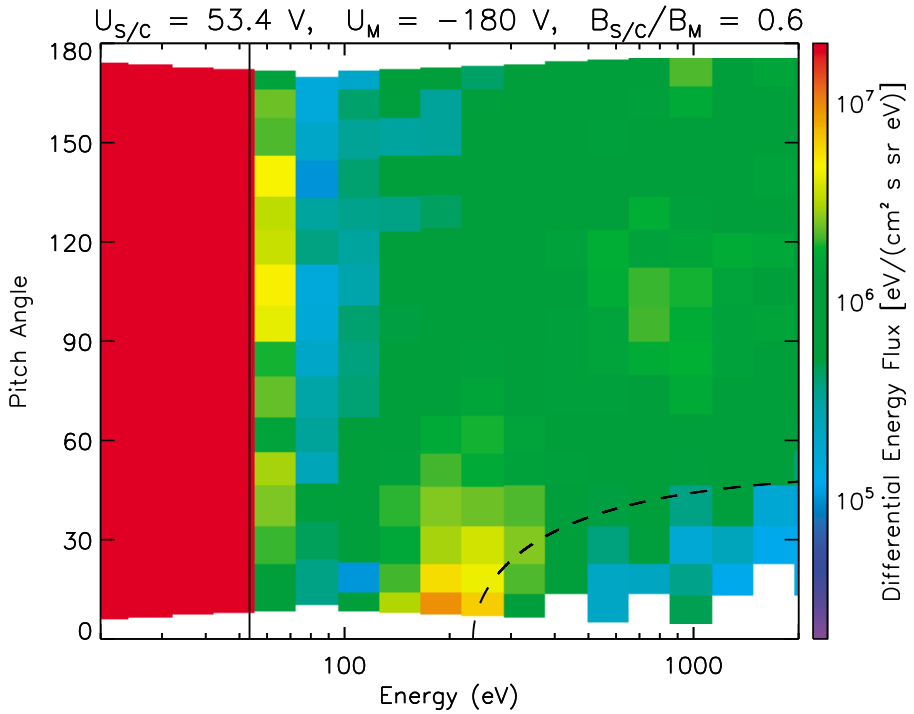

Figure 7. ARTEMIS-P2 electron data taken at 7:27:00, during a magnetically connected interval in the plasma sheet, in the same format as Figure 5.

velocity on the perpendicular ion spectra, showing that most of the energy of the cold ions corresponds to the field line convection velocity thereby inferred.

[24] Using this perpendicular velocity, and the known position of the Moon relative to the field line, we can calculate the time since a given field line would most recently have contacted the Moon (with zero values indicating connection, and negative values indicating field lines that should never have connected to the Moon). This analysis does not take into account field line curvature, and so provides only a first order estimate of field line motion past the Moon. Around the observed connection time, we see that the inferred field line motion undergoes rapid changes, resulting in intervals with predicted connection tens of seconds earlier, and intervals with no predicted previous connection. Obviously, this analysis, not taking into account the rapid rotations in field line direction (flapping) or field line curvature, can only provide an approximate answer. However, it at least provides a rough estimate of the order of magnitude of the time since magnetic connection to the Moon for an uncurved field line, on the order of tens of seconds. For comparison, a 400 eV electron can travel from the Moon to ARTEMIS-P2 in less than a second. Thus, we consider it highly implausible that travel time effects alone can explain the discrepancy between predicted and actual connection times for the entire ~30 s interval in question.

[25] Instead, fairly significant field line curvature (consistent with the location of the Moon in the plasma sheet, and the active plasma conditions and high Auroral Electrojet (AE) index during the observation time) likely must explain the observed discrepancy in connection times. As a result, we recognize that we cannot place very good constraints on the location of magnetic connection to the lunar surface during this interval, and indeed cannot rule out connection anywhere on the Moon (even including the night side), especially during the second half of the interval. However, given the inferred field line motion/rotation, corresponding to field line connection that sweeps across the Moon and back, by far the most likely scenario has the magnetic field line connected to the dayside surface for the majority of the connected interval.

5. Implications

[26] ARTEMIS, during this early lunar encounter, provided us with the first accurate and quantitative remote measurements of lunar surface charging. Intriguingly, negative dayside surface charging, very likely indicating nonmonotonic potentials above the sunlit surface, seems a ubiquitous feature of the lunar interaction in the magnetotail. Future lunar encounters, especially once the two ARTEMIS probes reach their final lunar orbits, should help characterize the effects of varying initial conditions, and the range of parameters for which nonmonotonic sheath potentials may exist. Already, though, we can examine two critical parameters, namely the electron temperature and the SZA of the field line foot point, in Figure 8. Clearly, the electron temperature controls the surface potential, with a roughly linear dependence, very consistent with previous predictions [*Poppe et al.*, 2011]. However, significant departures from this linear relationship exist, as shown in Figure 8 (bottom), with a suggestion of smaller negative potentials at lower SZA (especially if we make the ansatz that an interval for which a straight-line trace predicts no connection will tend to have magnetic connection to a portion of the surface with higher SZA). This SZA trend provides a testable prediction

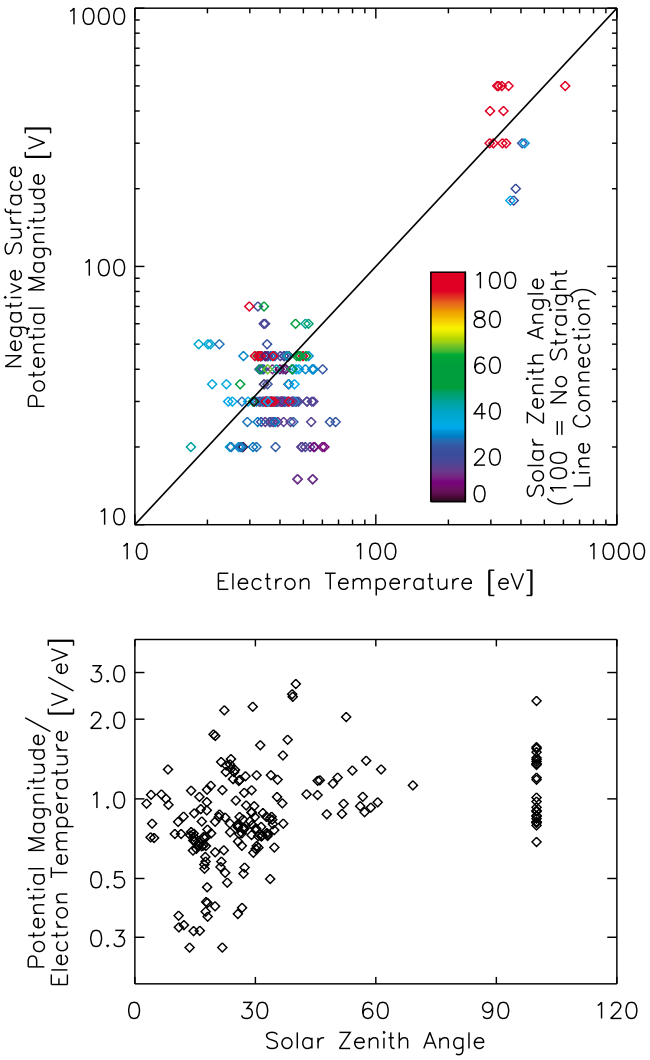

Figure 8. (top) Inferred magnitude of negative surface potential versus fitted moonward electron temperature for all data points in Figures 4 and 6, colored by the field line foot point solar zenith angle. (bottom) Ratio between magnitude of negative surface panel and fitted moonward electron temperature, as a function of foot point solar zenith angle. Red points (Figure 8, top), corresponding to points at SZA = 100 (Figure 8, bottom), indicate surface potential values inferred from earthward going electron beams measured at times when a straight line trace of the measured field vector does not intersect the Moon, likely indicating field line curvature.

for future modeling studies, and an interesting effect to look for from closer distances, where field line curvature cannot affect the results to the same degree.

[27] Future studies should also investigate the effects of crustal magnetic fields. During this interval, given the position of ARTEMIS and the Moon in the Earth's magnetotail and the phase-locked nature of the lunar orbit around the Earth, ARTEMIS encountered field lines connected to the lunar nearside, with a straight-line trace predicting magnetic connection to near-equatorial nearside lunar regions that have very few strong crustal fields. Given early indications from LP that crustal magnetic fields may strongly affect electric fields above the Moon in the solar wind [*Halekas et al.*, 2011], ARTEMIS measurements over regions with more significant crustal fields should prove very interesting.

[28] As discussed briefly by *Halekas et al.* [2011], the roughly linear dependence of negative dayside charging on electron temperature has some interesting implications. For instance, consider a magnetic field line moving laterally past the Moon. As that field line contacts the lunar surface, the Moon blocks incident plasma from one direction. Thus, absent a lunar source of plasma, a wing of reduced electron density should extend out from the Moon along the field line, with a rarefaction front traveling outward on the order of the electron thermal speed. In order to maintain quasi-neutrality, either electrons or ions must respond to compensate for this reduction in electron density, with electrons generally capable of reacting more quickly to neutralize charge buildups. Absent a source of lunar plasma, it remains unclear how this equilibration might proceed. However, given the high densities of electrons produced by photoemission from the lunar surface, the plasma can easily adjust by pulling a small fraction of the photoelectrons from this reservoir. In fact, a beam of electrons accelerated from the surface with an energy corresponding to the ambient electron temperature provides a source of electrons with exactly the properties needed to compensate for the outward traveling rarefaction front and maintain quasi-neutrality along the field line. Thus, the nonmonotonic potentials above the dayside lunar surface may in fact result at least in part from the requirement to maintain quasi-neutrality along magnetic field lines connected to the lunar surface.

[29] **Acknowledgments.** We thank the NASA Lunar Science Institute for supporting this work and acknowledge NASA contract NAS5–02099. FGM was supported by DLR contract 50 OC 0302. Financial support for the work of the FGM Lead Investigator Team at the Technical University of Braunschweig by the German Ministerium für Wirtschaft und Technologie and the Deutsches Zentrum für Luft- und Raumfahrt under grant 50OC1001 is acknowledged.

[30] Masaki Fujimoto thanks the reviewers for their assistance in evaluating this paper.

References

Anderson, K. A., and R. P. Lin (1969), Observations of interplanetary field lines in the magnetotail, *J. Geophys. Res.*, *74*, 3953–3968, doi:10.1029/JA074i016p03953.

Angelopoulos, V. (2010), The ARTEMIS mission, *Space Sci. Rev.*, doi:10.1007/s11214-010-9687-2, in press.

Auster, H. U., et al. (2008), The THEMIS fluxgate magnetometer, *Space Sci. Rev.*, *141*, 235–264, doi:10.1007/s11214-008-9365-9.

Bonnell, J. W., F. S. Mozer, G. T. Delory, A. J. Hull, R. E. Ergun, C. M. Cully, V. Angelopoulos, and P. R. Harvey (2008), The electric field instrument (EFI) for THEMIS, *Space Sci. Rev.*, *141*, 303–341, doi:10.1007/s11214-008-9469-2.

Ergun, R. E., D. M. Malaspina, S. D. Bale, J. P. McFadden, D. E. Larson, F. S. Mozer, N. Meyer-Vernet, M. Maksimovic, P. J. Kellogg, and J. R. Wygant (2010), Spacecraft charging and ion wake formation in the near-Sun environment, *Phys. Plasmas*, *17*, 072903, doi:10.1063/1.3457484.

Feuerbacher, B., M. Anderegg, B. Fitton, L. D. Laude, R. F. Willis, and R. J. L. Grard (1972), Photoemission from lunar surface fines and the lunar photoelectron sheath, *Proc. Lunar Sci. Conf.*, *3*, 2655–2663.

Freeman, J. W., and M. Ibrahim (1975), Lunar electric fields, surface potential and associated plasma sheaths, *Moon*, *14*, 103–114, doi:10.1007/BF00562976.

Guernsey, R. L., and J. H. M. Fu (1970), Potential distribution surrounding a photo-emitting plate in a dilute plasma, *J. Geophys. Res.*, *75*, 3193–3199, doi:10.1029/JA075i016p03193.

Halekas, J. S., R. P. Lin, and D. L. Mitchell (2005), Large negative lunar surface potentials in sunlight and shadow, *Geophys. Res. Lett.*, *32*, L09102, doi:10.1029/2005GL022627.

Halekas, J. S., G. T. Delory, R. P. Lin, T. J. Stubbs, and W. M. Farrell (2008), Lunar Prospector observations of the electrostatic potential of the lunar surface and its response to incident currents, *J. Geophys. Res.*, *113*, A09102, doi:10.1029/2008JA013194.

Halekas, J. S., Y. Saito, G. T. Delory, and W. M. Farrell (2010), New views of the lunar plasma environment, *Planet. Space Sci.*, doi:10.1016/j.pss.2010.08.011, in press.

Halekas, J. S., A. Poppe, G. T. Delory, W. M. Farrell, and M. Horányi (2011), Solar wind electron interaction with the dayside lunar surface and crustal magnetic fields: Evidence for precursor effects, *Earth Planets Space*, in press.

Hirahara, M., M. Nakamura, T. Terasawa, T. Mukai, Y. Saito, T. Yamamoto, A. Nishida, S. Machida, and S. Kokubun (1994), Acceleration and heating of cold ion beams in the plasma sheet boundary layer observed with GEOTAIL, *Geophys. Res. Lett.*, *21*, 3003–3006, doi:10.1029/94GL02109.

Manka, R. H. (1973), Plasma and potential at the lunar surface, in *Photon and Particle Interactions With Surfaces in Space*, edited by R. J. L. Grard, pp. 347–361, D. Reidel, Dordrecht, Netherlands.

McFadden, J. P., C. W. Carlson, D. Larson, M. Ludlam, R. Abiad, B. Elliott, P. Turin, M. Marckwordt, and V. Angelopoulos (2008), The THEMIS ESA plasma instrument and in-flight calibration, *Space Sci. Rev.*, *141*, 277–302, doi:10.1007/s11214-008-9440-2.

Nitter, T., O. Havnes, and F. Melandsø (1998), Levitation and dynamics of charged dust in the photoelectron sheath above surfaces in space, *J. Geophys. Res.*, *103*, 6605–6620, doi:10.1029/97JA03523.

Poppe, A., and M. Horányi (2010), Simulations of the photoelectron sheath and dust levitation on the lunar surface, *J. Geophys. Res.*, *115*, A08106, doi:10.1029/2010JA015286.

Poppe, A., J. S. Halekas, and M. Horányi (2011), Negative potentials above the day-side lunar surface in the terrestrial plasma sheet: Evidence of nonmonotonic potentials, *Geophys. Res. Lett.*, *38*, L02103, doi:10.1029/2010GL046119.

Reasoner, D. L., and W. J. Burke (1972), Characteristics of the lunar photoelectron layer in the geomagnetic tail, *J. Geophys. Res.*, *77*, 6671–6687, doi:10.1029/JA077i034p06671.

Tanaka, T., et al. (2009), First in situ observation of the Moon-originating ions in the Earth's magnetosphere by MAP-PACE on SELENE (KAGUYA), *Geophys. Res. Lett.*, *36*, L22106, doi:10.1029/2009GL040682.

Whipple, E. C. (1981), Potentials of surfaces in space, *Rep. Prog. Phys.*, *44*, 1197–1250, doi:10.1088/0034-4885/44/11/002.

Willis, R. F., M. Anderegg, B. Feuerbacher, and B. Fitton (1973), Photoemission and secondary electron emission from lunar surface material, in *Photon and Particle Interactions With Surfaces in Space*, edited by R. J. L. Grard, pp. 389–401, D. Reidel, Dordrecht, Netherlands.

V. Angelopoulos, Institute of Geophysics and Planetary Physics, University of California, Los Angeles, CA 90095, USA.

J. W. Bonnell, G. T. Delory, M. O. Fillingim, J. S. Halekas, and J. P. McFadden, Space Sciences Laboratory, University of California, 7 Gauss Way, Berkeley, CA 94720, USA. (jazzman@ssl.berkeley.edu)

W. M. Farrell, NASA Goddard Space Flight Center, Greenbelt, MD 20771, USA.

F. Plaschke, Institut für Geophysik und Extraterrestrische Physik, Technische Universität Braunschweig, Braunschweig D-38106, Germany.